Spectral broadening in tight-confinement geometry of a random fiber laser

A. R. SARMANI[1*], A. W. AL-ALIMI[2], N. MOHD YUSOFF[3,4], AND M. A. MAHDI[3]

[1]Department of Physics, Faculty of Science, Universiti Putra Malaysia, 43400 UPM Serdang, Selangor, Malaysia
[2]Department of Electronic Engineering, Faculty of Electrical and Electronic Engineering, Universiti Tun Hussein Onn Malaysia, 86400 Batu Pahat, Johor, Malaysia
[3]Wireless and Photonics Networks Research Centre, Faculty of Engineering, Universiti Putra Malaysia, 43400 UPM Serdang, Selangor, Malaysia
[4]inLAZER Dynamics Sdn. Bhd., InnoHub Unit, Putra Science Park, Universiti Putra Malaysia, 43400 UPM Serdang, Selangor, Malaysia
**abd_rahman@upm.edu.my*

Abstract: We present a random Raman fiber laser pumped by a continuous-wave 1480nm source where neither a visible saturable absorber nor a fiber Bragg grating were incorporated. The backward pumping feedback loop allows a single direction of 1584nm wave propagation under tighter confinement of a dispersion compensating fiber (DCF). This geometry that implies a stronger Kerr-lensing effect supports two types of nonlinear broadening that were achieved in the stable output power generation. The first that agrees well to wave kinetics theory favors 1.76 to 3.53nm spectral progress. Against this flow, another type of wider broadening begun at 4.88nm before reducing gradually to 4.05nm with the increase in pump power. The former corresponds to a maximum of 6.3 times broadening ratio with respect to the pump linewidth. To date, this is the best achievement in the world at just below 1.7 W pump power level especially without utilizing pump-pulse synchronization or any external mode-locking modulations. In contrast without the tighter confinement geometry, the initiation of 4.25nm bandwidth was realized in the unstable power zone. These ascertain the double roles of dispersion compensating fiber as a stabilizing factor as well as for dispersion management.

Index Terms: Random fiber lasers, Fiber non-linear optics.

1. Introduction

The first impressive breakthrough on random Raman fiber lasers (RRFL) in ultralong fibre strands that were built in open cavities were accomplished in 2010 [1, 2]. In spite of the fact that no any regular reflector was used, the conventional lasing principles namely spectral characteristics [3], threshold [4] and wavelength tunability [5] still apply. The overall performances were comparable to regular lasers where a stationary near-Gaussian beam with a narrow spectrum was generated. These were obtained owing to the cylindrical fiber waveguide structure that offers two advantages. The first is transverse confinement and the second is efficient one-dimensional random distributed feedback. The first aspect allows a high-intensity intracavity light propagation that results in a strong stimulated Raman scattering (SRS) transition. This is further supported by very small core diameter of less than 10μm and low loss coefficient of ~ 0.2dB/km at 1550nm. Moreover the second aspect is as a result of multiple Rayleigh backscattering (RBS) in the longitudinal dimension that is induced by the fiber inhomogeneities that imply refractive index fluctuations. Although the influence of RBS in the fiber core is extremely negligible, it is accumulated efficiently over a very long distance. In the last few decades, the simple and stable sources of RRFLs have been very well constructed in numerous configurations. Together with overviews on their cutting-edge

Preprint not peer reviewed

This preprint research paper has not been peer reviewed. Electronic copy available at: https://ssrn.com/abstract=4184332

progressess, theoretical developments and perspectives are all summarized in [6, 7]. Both references also gave elaborations on great potentials of these sources for practical applications, namely narrow-linewidths, telecommunications, distributed optical sensing and multiwavelength generation.

With regards to wide developments in this area, studies on spectral and statistical properties, wave kinetics, optical nonlinearities, high power as well as other lasing characteristics were done [3, 8-18]. In [9], both the spectral narrowing and broadening theories described well the experimentally measured laser linewidths at all power scales. These behaviors are almost equivalent to those elaborated versus pump power (see Fig. 2 in [3]). In addition to all descriptions at first order Stokes-waves [3, 8-17], progresses were also accomplished at those of the second [10, 13, 14] and third-order Stokes [13] by utilizing narrow band continuous-wave, CW as well as broadband ASE pump sources. In all these assessments, the nonlinear broadening was more influential at higher power generation. This is further supported in the systems that consist of larger Kerr-nonlinearity, γ and smaller fiber dispersion, β_2. Upon the appropriate control between both criteria resulted in the simulation of 2.6nm FWHM. The modelling was first discussed in 2013 [18] and up to now no comparison to any experimental finding could be done, thus opens-up more opportunities in the next time to come. Similarly, the phenomenon that is known as turbulence-induced broadening was also reported by S. A. Babin and associates in conventional Raman fiber laser architectures [19-21]. In all these cases [1-21], phonon vibration of stimulated Raman scattering (SRS) in optical fibres is utilized. This is because amongst the lasing material bases, the main drawback associated to rare earth doped gain media is limited spectral emissions depending on the cavity resonance. Once this is overcomed at any selection of pump waves available, lasing peaks that correspond to 13THz. Raman shift can be generated in silica hosts. Thus, covering the region unattainable in the ionic based transitions.

Therefore in this manuscript, we demonstrate the performances of an upgraded version of RRFL in a linear cavity. Neither a fiber Bragg grating (FBG) that functioned as a spectral selective element nor a passive mode-locking component were inserted to the oscillator which differ to those utilized in [3, 8, 15]. The exclusion of the former device eliminates any spectral restriction on the bandwidth development and this is feasible by taking into account that the continuous modeless spectrum is free of SRS mode competition. A combination of SMF-28 and Truewave plus (TW+) fibers were utilized as the gain media. Unlike those used in [22, 23], the most striking element was the implementation of a narrow linewidth, CW Raman pump unit (RPU) without external self-modulation or synchronization. The key point was the single direction of light feedback under tighter confinement of dispersion-compensated fiber (DCF) that introduces optical Kerr nonlinearity, γ. This concept has been very well developed in solid-state lasers, SSL [24, 25]. For testing this idea in this work, the experiment was also repeated briefly with the exclusion of DCF. From the practical aspect, the indication for efficient exploitation of γ in this setup is confirmed with more than 4nm lasing bandwidth completion at very low power operation. A promising outlook is anticipated for revealing SSL trait in the random lasing nature once sufficient understanding of this technique is reached. As some of the fundamentals still can't be explained well yet, we only focus on reporting experimental results without too much concerning on the comprehensive theoretical backgrounds and simulations. In addition, the principal motivation behind the extended wavelength research direction towards L-band and higher was the relatively eye-safer applications. These range from medicine, biophotonics and environmental sensing to free-space optical communications and defense industry.

2. Experimental Details

The asymmetrical design of the random laser is illustrated in Figure 1. It was pumped by a CW, single-mode Raman pump unit (RPU) at 1480nm wavelength. The RPU has a beam

Preprint not peer reviewed

This preprint research paper has not been peer reviewed. Electronic copy available at: https://ssrn.com/abstract=4184332

quality, M^2 of 1.1 and provided a maximum pump power of 1690mW. The linewidth was around 0.77nm and the power fluctuation over an hour duration was less than ±1mW. This power was arranged for 100% backward pumping, P_b by splicing directly to the pump port of a 1480/1550nm wavelength division multiplexer of WDM2. No any power was delivered to WDM1 and its corresponding pump port was angled-cleaved to introduce 14dB isolation. This was responsible to prevent any Fresnel back reflection light to the setup. The gain media employed in this laser scheme were a 14km SMF-28 (SMF) and a strand of 32km True-wave plus fiber (TW+) obtained from OFS. This was done based on the resource availability in the laboratory. The SMF has a mode-field diameter (MFD) of 10.4 ± 0.5μm at 1550nm with a Raman gain coefficient (g_R) around 0.45(Wkm)$^{-1}$. In comparison, the TW+ fiber that has a higher value of g_R up to 0.6(Wkm)$^{-1}$ implies a MFD of 8.4 ± 0.4μm at the same wavelength range.

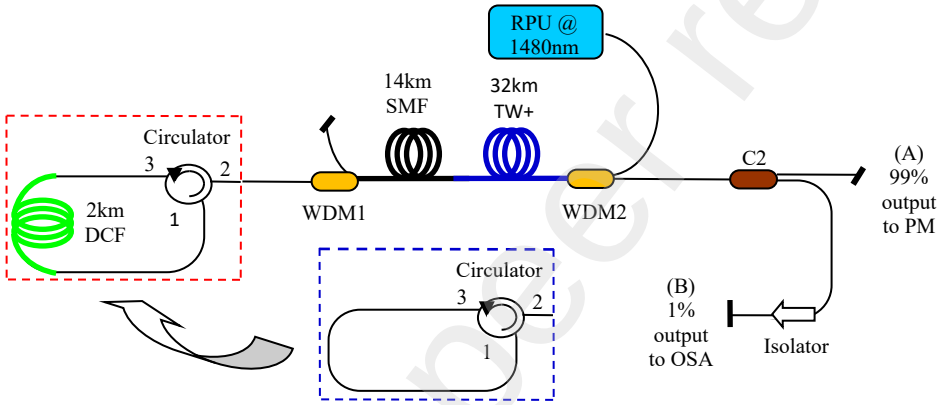

Fig. 1. Layout of a backward-pumped RRFL with the feedback loops in the dashed boxes.

In fact with the exclusion of FBG's, two types of unidirectional feedback loop were implemented as depicted in the dashed boxes in Fig. 1. These were a single-pass (SP) beam propagation from port 3 to port 1 of a circulator in a counter-clockwise direction. This type of beam propagation was arranged to ensure efficient wave kinetic response in a single-transmission line that is responsible for spectral broadening. For the red-dashbox, a 2km dispersion-compensated fiber (DCF) was included. This has an effective area of 20μm^2 with a nonlinear coefficient, γ of 7.31(Wkm)$^{-1}$. Due to mismatches between all these fiber dimensions, splicing losses were minimized to ≤ 0.6dB without the utilization of any taper scheme. To compare the output of lasing features at different fiber nonlinearities, the DCF was removed. No any additional ultralong fiber intermedium was utilized as the beam transmitted directly from port 3 to port 1 of the circulator. This is manifested in the blue-dashbox in Fig. 1 where both types of configurations are elucidated in Table 1. From this table, setup 1 represents the utilization of DCF in the feedback loop. With no any extra fiber intermedium, setup 2 is used for identification.

With reference to Table 1, both setups induced net anomalous dispersion that was not optimized to 0. This sum was deduced from the dispersion value for each fiber as summarized in Table 2. Besides this, the signal port of WDM2 that has an operating range of 1528 to 1610nm was coupled to a 99/1 coupler, C2. This operating property ascertained that only the first-order Raman-shift was detected with the minimum presence of any higher-order series. Along with the feedback loop, the completion of the laser cavity was realized through distributed Rayleigh-scattering inside the ultralong gain media. This was supported by

Preprint not peer reviewed

This preprint research paper has not been peer reviewed. Electronic copy available at: https://ssrn.com/abstract=4184332

terminating the 99% output port of C2, labeled as port (A) with an angle-cleaved fiber. The lasing transition was at a peak of 1584nm wavelength that relates to 13THz SRS shift in the silica fiber. The output power and its stability were measured by using a power meter (PM) located next to port (A) in a free-space arrangement. In addition, the spectral behaviors from 1% output of C2 (port B) was monitored by utilizing an optical spectrum analyzer (OSA). This equipment was set at its best 0.06nm resolution and the relevant fiber-end has a flat-angled property. In this fiber-coupled contact, the propagation of Raman photons in only a single direction was secured with the employment of an isolator that has 56dB isolation.

Table 1. Fiber arrangements as outlined in Fig. 1.

Setup	Gain Media	Feedback loop	Net group velocity dispersion, GVD (ps^2)
1	14km SMF and 32km TW+	2km DCF (tighter geometry)	-240.07
2	14km SMF and 32km TW+	SMF Fiber (ordinary geometry)	-547.82

Table 2. Estimated dispersion values at 1584nm wavelength in each fiber used in this assessment.

Fiber type	Dispersion @ 1584nm (ps/nm.km)	$\beta_2 = \frac{D\lambda^2}{-2\pi c}$ @ 1584nm (ps^2/km)
SMF-28	19.49	-25.94
Truewave plus (TW+)	4.34	-5.77
Dispersion compensating fiber (DCF)	-115.6	153.88

3. Results

In [3], efficient nonlinear broadening was observed when applying 100% forward pumping. However with this kind of pumping without any Bragg grating in the laser design outlined in Fig. 1, the lasing was disrupted by cascaded Brillouin transition lines and dual wavelength oscillations. As a consequence, only a small power region was dominated by a single-wavelength lasing. This justifies the favorable selection of 100% backward pumping in this report where the single-wavelength lasing prevailed in almost the entire operation. The main objective of this work was to study the dynamics of spectral broadening at 1584nm operating wavelength by applying tight-confinement in the fiber dimension of random laser.

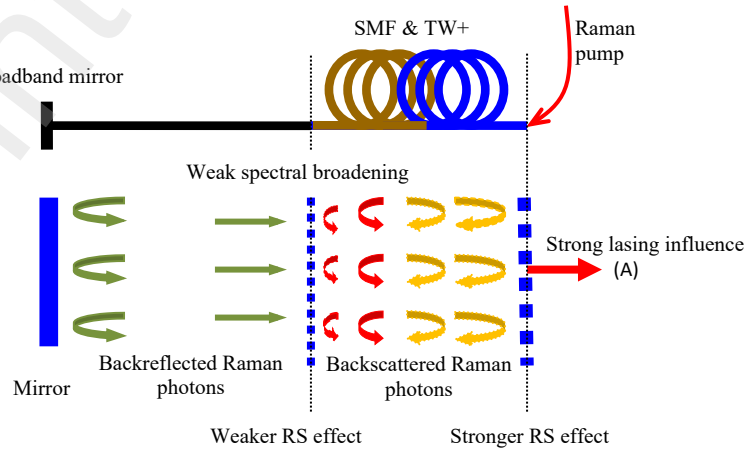

Preprint not peer reviewed

This preprint research paper has not been peer reviewed. Electronic copy available at: https://ssrn.com/abstract=4184332

Fig. 2. Microscopic Raman photon propagation in the 100% backward-pumped RRFL constructed in Fig. 1.

Before starting any experiment, the basis behind Raman waves interactions in this advanced setup should be understood first. The simplified diagram is shown in Fig. 2 where the feedback loop is replaced by a broadband mirror. In theory, wave kinetics [9] induced by net accumulations of strong backreflected waves originating from the mirror only happens in one direction. A significant broadening implies the dominance of these backreflected waves supported by backscattered Raman photons when propagating together towards the output port (see Fig. 5 in [3]). This is followed by saturation of the output power as most energy is utilized to compensate the energy conversion required for nonlinear broadening (see Fig. 4 in [3]). In contrast, its smaller bandwidth attainment signifies the struggle of these backreflected waves (green arrows) over the opposite direction of backscattered Raman photons emerging from the backward pumping waves (orange arrows). This is depicted in Fig. 2 and as a consequence, a stronger distributed virtual mirror is introduced at port A. Therefore together with the assistance of the broadband mirror that completes the laser cavity, most of the energy is consumed to produce higher lasing power instead of assisting the spectral growth. This justifies the insight behind weak generation of wave kinetics when specifically implementing this kind of pumping-arrangement (see Fig. 2 and 3 in [3]). The "weak" terminology is just a relative definition when referring to a more efficient nonlinear response in 100% forward pumping (compare Fig. 2 and 4 in [3]). However, this is already adequate to initiate early studies on FWHM growth with further prospects of improvements in the future endeavors.

Once the principles above are understood, detail studies on various lasing modes particularly in the nonlinear broadening regimes are presented. The bandwidths were evaluated by considering the full-width at half maximum, FWHM and we only focus on the important developments since some elaborations have been covered in the past reports [3, 8, 9]. In random lasing, it was very difficult to differentiate the boundary between CW to other types of operation especially mode-locking owing to the modeless interacting waves. To resolve this issue, there were a few states that we described ourselves depending on the bandwidth values. The first was beyond 4nm lasing band that is identified as wider spectra, "WS" and the second was spectral broadening effect "SBE", both are discussed in setup 1. The first-state was realized by immediate spectral increase at a certain pump power level as depicted in Fig. 3. This was recognized by a sound "click" that also implies a switching power transformation as a substantial output power drop was produced, we didn't know the insights behind this audible initiation as the main aim was only to report the observation. All of these occurred synchronously in the stable power region. However, no any audio was heard at the end of its performance that was represented by immediate bandwidth reduction accompanied concurrently by a significant increase in output power. For the second state of "SBE", the bandwidth expanded slowly from 1.76 nm up to 3.53nm range as proven in Fig. 3. The flow almost satisfies the weak wave kinetics theory as outlined in Fig. 2 where no audio change to signalize its initial and end-phases. Sometimes a wider spectral regime was characterized as "UWS" in Fig. 7 where character "U" denotes its occurrence in the unstable power zone. As output power fluctuations were developed in this case, the bandwidth widened and shrunk accordingly at the same time which clarifies the hardship to complete the measurements.

Throughout experiment, the RPU pump power that was stable at all levels within ±1mW was increased gradually up to 1 decimal point. The lasing behaviors namely output power and its stability in the corresponding pump power domain were observed carefully between 3 to 5 minutes. All data shown in Figures 3 to 7 fell in the stable regimes that correspond to output power variations within ± 1mW. The unstable power performance, namely the "UWS" state is only presented in Fig. 8 together with its specifications in Table 3. At both laser setups (Fig. 3

Preprint not peer reviewed

This preprint research paper has not been peer reviewed. Electronic copy available at: https://ssrn.com/abstract=4184332

and 7), stimulated Brillouin scattering (SBS) lines were sometimes observed on the Raman gain bandwidth near threshold. This led to instability of the CW regimes as manifested by unstable generated power. Despite of this, the Raman gain transition dominated over the SBS lines with the increase in power generation above threshold. This indicates the total removal of gain competition between both nonlinearities during random lasing especially when implementing full backward pumping arrangement (Fig. 1). Once this was attained, improvements to the output power stability were realized which was similar to that elaborated in [1]. Moreover the utilization of a CW, single-mode RPU in this experiment indicates no requirement for a multimode pump source to suppress the SBS generation in conventional designs [26, 27]. This shows some of the advantageous nature of random lasing mechanism. Thus to understand this physical concept, the quality of spectral broadening is elaborated.

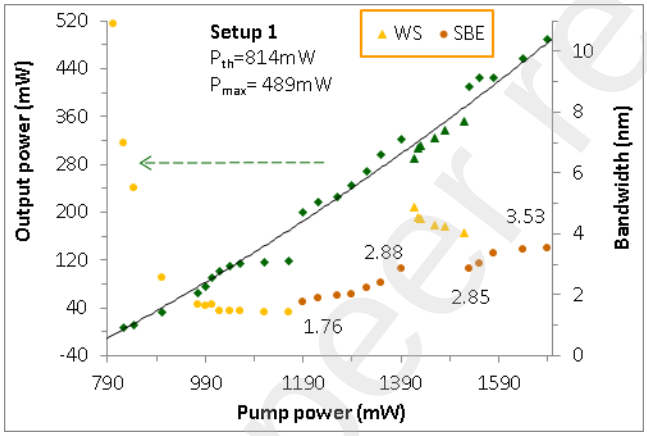

Fig. 3. Lasing characteristics against pump power. Triangle plots: "WS" state at P_p of 1417.6 to 1529.8mW (WS: wide spectra, SBE: Spectral broadening effect, P_p : pump power).

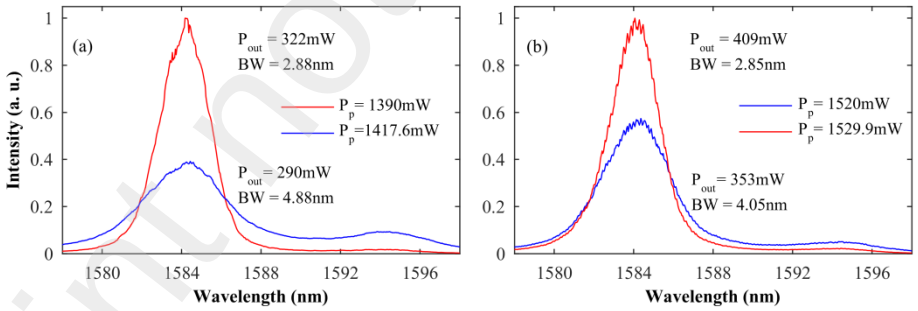

Fig. 4. "WS" (blue line) versus "SBE" spectra (red line) for setup 1 in (a) that shows the beginning and in (b) for its corresponding end-state.

Preprint not peer reviewed

This preprint research paper has not been peer reviewed. Electronic copy available at: https://ssrn.com/abstract=4184332

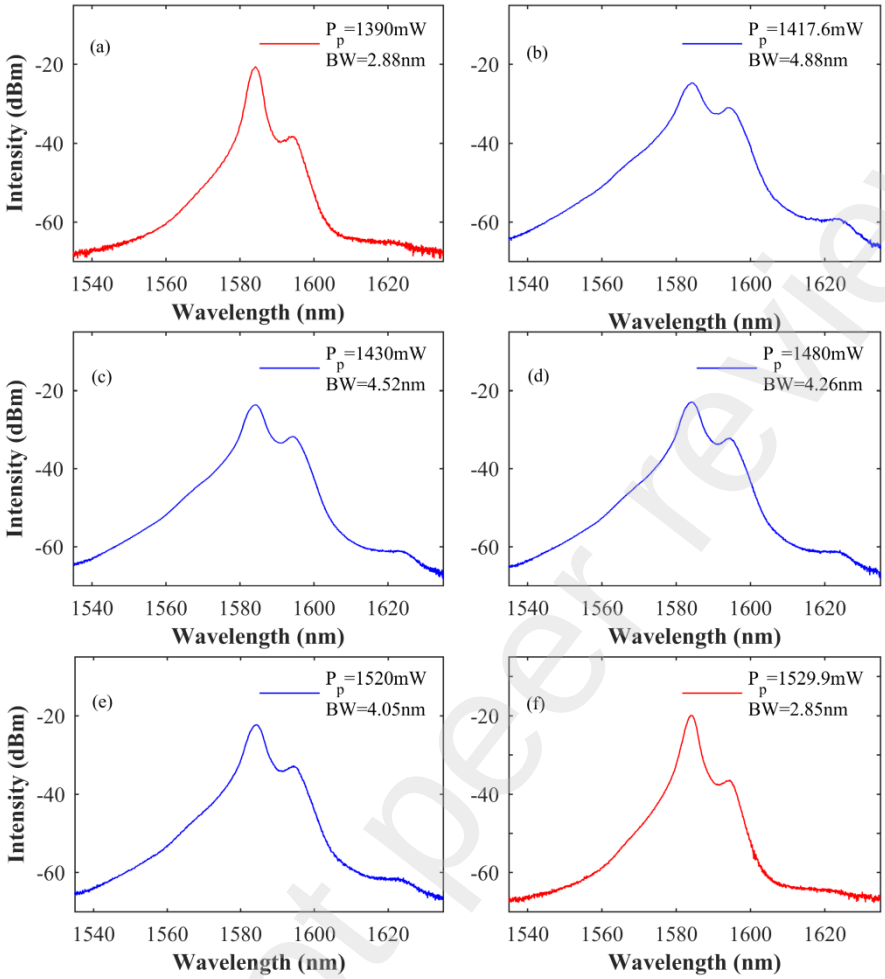

Fig. 5. "WS" (blue lines) against "SBE" spectra (red lines) in dBm peak power similar to Fig. 4.

At the outset of this assessment, the results of output power and bandwidth progressions for setup 1 are presented in Fig. 3. A power threshold, P_{th} of 814mW was satisfied from the quadratic curve of the lasing plot (black line). Initially two output power plots at 116 and 118mW (green diamond) at the end spectral narrowing region (orange circle) deviated from the lasing trendline before jumping up to 199mW when the pump power was set to 1190mW. This might be because the Raman energy was not enough to compensate some losses introduced by the DCF until certain pump power was achieved. After this level, the power almost complied with the nonlinear quadratic fit without showing any saturation sign which is in consistency to that described earlier (see Fig. 2 in [3]). Maximum output power, P_{out} of 489mW was attained that yields 29% optical-to-optical efficiency with respect to the pump power. Simultaneously, the bandwidth development was also inspected thoroughly on the OSA. Both settings for video bandwidth, VBW. of 2.1kHz and sensitivity, Sens. of -65dBm were maintained at the same levels for the entire operation. In particular, the main topics of interests are namely on "WS" and "SBE" regions that are illustrated in Fig. 4 to 6. Below threshold, the spectral envelope consisted mainly of amplified spontaneous emission (ASE) that explained a wide bandwidth development of more than 10nm. Once lasing begun, the spectral wing envelopes were slowly dominated by stimulated Raman transitions that were responsible for the narrowing effect (orange circle). The beginning state of "SBE" was

Preprint not peer reviewed

This preprint research paper has not been peer reviewed. Electronic copy available at: https://ssrn.com/abstract=4184332

realized at 1190 mW pump power where the bandwidth increased to 1.76nm (brown circle). This signifies the weak initiation of wave kinetics (Fig. 2) as the optical bandwidth expanded slowly to 2.88nm with the continuous increment in pump power domain up to 1390mW. Both bandwidth behaviors were found to be in accordance to the predicted theories (see Fig. 3(b) in [9]).

Unpredictably beyond the physical concept outlined in Fig. 2, when the pump power P_p was enhanced slightly from 1390 to 1417.6mW a noticeable "WS" regime was started (Fig. 3). Almost 32mW output power drop was measured within this small order of pump power increase. A sound "click" was also heard together with the concurrent commencement of 1.7 times wider spectrum. This is demonstrated by the blue profile in Fig. 4(a) where the maximum bandwidth, BW of 4.88nm was produced. The P_{out} was 290mW that relates to 20.5% optical-to-optical-efficiency η. The central wavelength was at 1584.2nm where the "WS" state was stable. The distinctive "WS" regime only covered a small pump power portion from 1417.6mW to 1529.8mW as represented by triangle plots in Fig. 3. At 1520mW pump power, a spectral width of 4.05nm was measured at a central wavelength of 1584.1nm [Fig. 4(b)]. The P_{out} was 353mW that corresponds to η of 23.2%. We need to stress that very careful observation was performed with the gradual increment in the pump power where the "WS" signal was still in effect at P_p = 1529.8mW although this was not recorded. Just a minor increase in the pump power to 1529.9mW resulted in nearly 1.4 times bandwidth constriction. This is depicted in Fig. 4(b) when the blue spectrum evolved into that of the red one. Synchronously, this was followed by a substantial increase of 56mW output power which signified the end of this state. As a result, the output power improved drastically to 409mW with a smaller FWHM of 2.85nm. The complete representation of Fig. 4 in dBm peak power is demonstrated in Fig. 5. The main idea of showing the latter diagram is to prove that the "WS" state was primarily induced by CW spontaneous radiation without fluctuations or Q-switching instabilities at the band edges. From both figures as no any Bragg reflector was placed inside the cavity to discriminate lasing at another peak wavelength, a secondary peak around 1594nm was observed. It was more pronounced in the "WS" modes due to the stronger broadening in comparison to that in other modes. Besides this, the transition between "SBE" to "WS" and vice versa as shown in Fig. 3 is not understood well yet owing to our lack of expertise and facilities. In addition, as no any external mode-locking modulations as explained in [15, 22, 23] were inserted to this cavity-free structure, no ultrashort pulses that become the subject of our main interest were detected similar to that assessed earlier (see Fig. 5 in [17]). The pre and post "WS" state that was classified as "SBE" almost satisfied the weak wave kinetics signature as described in Fig. 2. This is owing to the overall bandwidth development from 1.76 to 3.53nm as manifested in Fig. 3 (brown circles). Other spectral changes with the absence of "WS" signals are depicted in Fig. 6. Although minor ripples were the feature for "SBE" category, smoother beam curves were the typical attribute at a lower power segment ($P_p \leq 1160$mW). From this figure also the precise central wavelength, λ_c that begins at 1583.13nm shifted 1.38nm to the right with the increase in P_p from 843 to 1690mW. The main reason is believed due to thermal effects (see Fig. 2(b) in [29]) which explains the generation of asymmetrical spectral shapes in the previous assessment (see Fig. 2(a) in [3]).

From [3] that demonstrates a 100% forward pumping layout, the pumping enhancement up to 1585mW led to the maximum bandwidth of 0.9nm. This is almost 2.8 times wider compared to the 3dB reflection band of the FBG. In the similar pumping arrangement, the spectral broadening from 0.11 to 0.96nm was developed with the pumping increment from 14mW to 2.88W [15]. In other assessments, spectral broadening at the first Stokes wave emission was lower than 1.8nm [9-14]. The spectra were limited to below 2.6nm and 3.5nm at

Preprint not peer reviewed

This preprint research paper has not been peer reviewed. Electronic copy available at: https://ssrn.com/abstract=4184332

second-Stokes [13, 14] and third-Stokes components [13], respectively. These indicate that above 1.76nm FWHM could only be fulfilled in the CW-pumped [3, 9-13, 15] and ASE-pumped RRFLs [14] at higher-orders with multiple Watts output power generation. The exception to this bandwidth rule was observed in later advancements at 1st-Stokes order [16, 17]. A stable statistical mean value of 14nm spectral width was achieved in an open cavity RFL, but this is only a ratio of 0.875 to the linewidth of the incoherent ASE pump source [16]. Although up to a maximum of 7.31nm spectral width was attained in [17] but it is only 3.8 times wider compared to the reflection bandwidth of the FBG. Both results also necessitate high output power scaling from below 10W [16] to over 200W levels [17]. Nevertheless, the superior low power laser design of setup 1 was proven for better applications that favor nonlinear broadening at the fundamental Stokes waves emission from 1.76 up to 4.88 nm range. The latter implies exceptionally 6.3 times more expansion than the linewidth of the pump source where no any spectral selective element was employed. This report represents the best broadening proportion in any CW and ASE pumping based random fiber lasers at just within hundreds mW output power levels. In fact this claim is justified by taking into account that no pump-pulse synchronization or external mode-locking modulations were used as incorporated in past attempts [15, 22, 23].

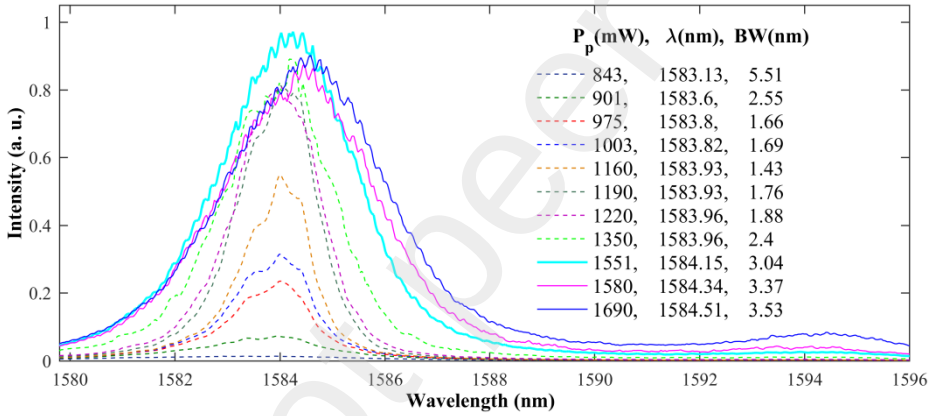

Figure 6. Spectral features in narrowing and "SBE" regions as described in Fig. 3. No "WS" beam curves are included. (λ_C : central wavelength, BW: bandwidth).

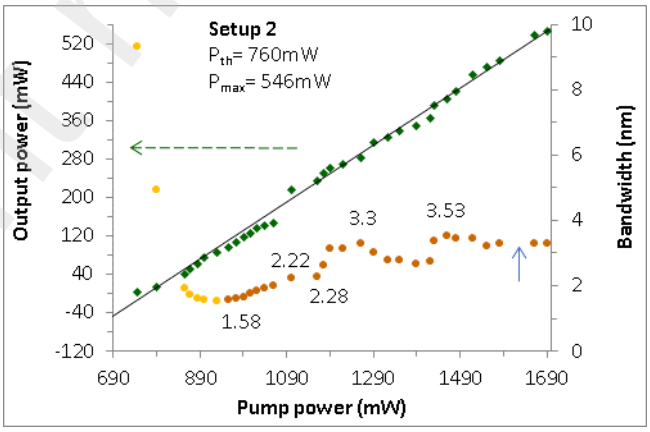

Fig. 7. Lasing properties against pump power. Blue arrow: "UWS" state at P_p of 1587.4 to 1661.4mW. (UWS: unstable wide spectra, P_p : pump power).

Preprint not peer reviewed

This preprint research paper has not been peer reviewed. Electronic copy available at: https://ssrn.com/abstract=4184332

Next, the results for setup 2 that comprised no DCF (Table 1) are illustrated in Fig. 7. The threshold power P_{th} of 760mW was satisfied where the output power plot conformed to the linear trendline estimation (black line) without any apparent deviation. This is in contrast to the quadratic power behaviors in the prior setup. In addition, no series of "WS" state and its corresponding power drop and rise from the linear fit was initiated. For the bandwidth study, we concentrate only on the development beyond 957mW pump power as represented by the brown circles. Initially, smooth broadening transition was observed from 1.58 to 2.22nm. This was followed by an inconsistent flow from 2.28 to 3.3nm range at the middle power scheme. Another segment above 1429mW pump power also did not obey the wave kinetics owing to saturation as most of the energy was used for the conversion to higher lasing power. Nevertheless, the maximum BW in this power portion is similar to that obtained in Fig. 3. No stable "WS" state was realized but the unstable one, "UWS" was achieved in the P_p segment that is denoted by the blue arrow in Fig. 7. It should be acknowledged again that all P_p levels were stable within ±1mW estimation at all time. It was the respective output power that fell in unstable regimes. Therefore, it was very difficult to observe the significant P_{out} drop and increase from the linear fit that signify the beginning and end of this characteristic. Without the tight DCF geometry, the scheme was struggling to control its stability. The depictions on this behavior are given in Fig. 8. Prior to this, the initial BW was 3.3nm at P_p = 1580mW before undergoing broadening that reached a maximum up to 4.25nm at P_p of 1587.4mW. This is the widest record that we managed to acquire manually because the formation and the elimination of "UWS" state took place immediately at the same time. The FWHM was narrower than that obtained in the previous setup and this is expected by referring to the net GVD listed in Table 1. The process started from the initiation of q-switching instability as manifested by the band-edges of a few signals in Fig. 8. Our main aim was not to measure the pulses and peak power initiated by Stimulated Brillouin Scattering, SBS as this has been detailed in [30]. In addition to power fluctuations, the spectral widths also kept changing and both properties are described in Table 3. Sometimes narrow linewidth Brillouin lasing lines popped-up "ON" and "OFF" on the lasing spectra. The BW continued to decline with the continuous pumping in a similar behavior to the triangle plots in Fig. 3. In comparison to "WS" state, the categorization of "UWS" did not only depend on above 4nm lasing bandwidth definition. This also included the dynamics of indispensable q-switching response observed on the lasing signals that thwarted further broadening. Owing to this reason, the inconstant signals below 4nm-order are still classified in "UWS" category [see Fig. 8(c to e)]. This was totally terminated when the pumping was enhanced to 1661.5mW. The FWHM was reduced to 3.31nm together with stabilization in output power to 538mW. To avoid any confusion, it should be emphasized again that the data in the stable region is presented in Fig. 3 to 7 and the unstable data denoted by the blue arrow in Fig. 7 is specified only in Fig. 8 and Table 3.

Preprint not peer reviewed

This preprint research paper has not been peer reviewed. Electronic copy available at: https://ssrn.com/abstract=4184332

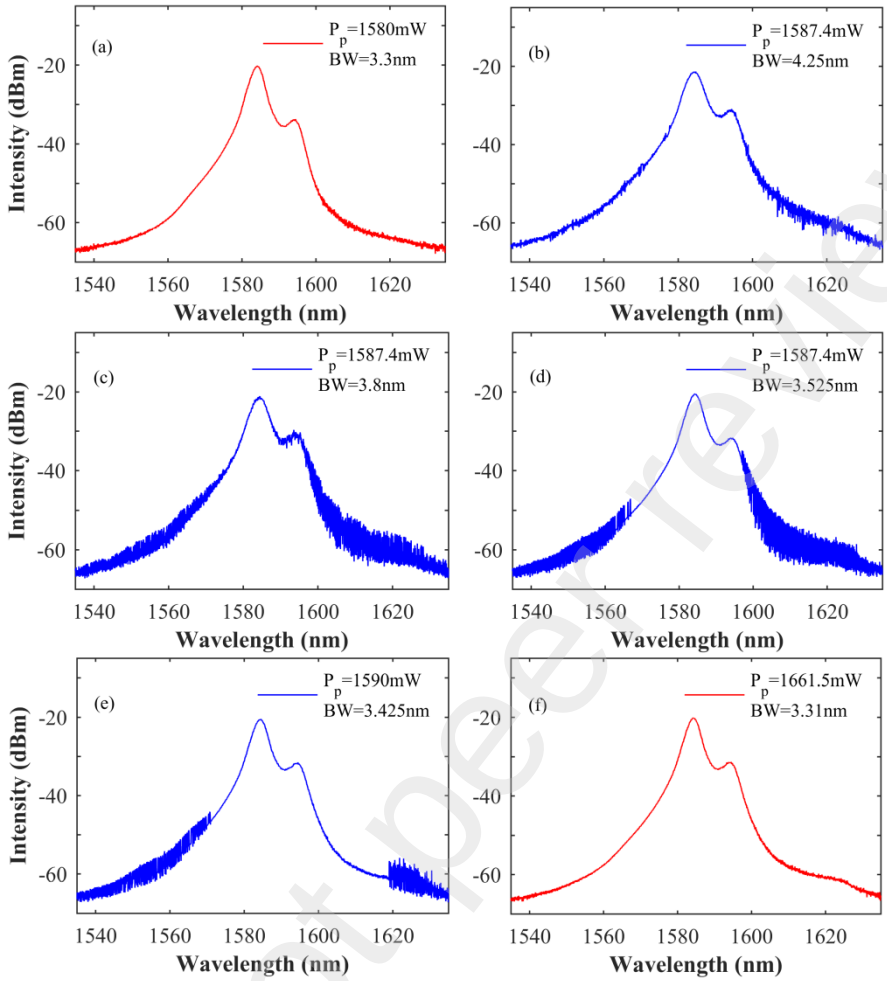

Fig. 8. "UWS" (blue lines) against other spectra (red lines) in dBm peak power that demonstrate the fluctuations of spectral width at 1587.4mW P_p as described in Table 3.

Table 3. "UWS" state properties in setup 2.

Lasing state	P_p (mW)	P_{out} (mW)	BW (nm)
Stable mode	1580	484 ± 1	3.3
UWS	1587.4	494 ± 7	Fluctuates from 4.25 to 3.525
UWS	1590	502.5 ± 3.5	Fluctuates around 3.425
UWS	1625	518.5 ± 19.5	Fluctuates around 3.425
Stable mode	1661.5	538 ± 1	3.31

For concise explanations, the summaries are presented in Table 4 below. As references in [3-5, 8] verified the similar behavior between random lasing to that of a conventional one, we assume that a reasonable analogy to Kerr-lensing effects in solid-state

Preprint not peer reviewed

This preprint research paper has not been peer reviewed. Electronic copy available at: https://ssrn.com/abstract=4184332

lasers [24, 25] can be drawn between both lasing criteria. From the experimental setup (Fig. 1), the pump beam mode is restricted in the gain medium owing to the filtering scheme introduced by two WDMs (WDM1 & WDM2). The residual pump light is removed out through the corresponding port of WDM1. With the formation of virtual cavity during lasing, the laser beam mode propagates in the entire oscillator and overlaps with the pumping mode in the gain medium. The smaller core DCF provides assisted reshaping of the laser beam diameter as a function of intensity along the fiber longitudinal dimension. The purpose is to facilitate self-focusing and efficient gain guiding influences that afford an improved overlap (mode-coupling) between the laser beam and the pump mode volumes. Owing to this, the reduction of the beam spot size is realized that serves to enhance the radial and temporal-dependent intensity, $I(r,t)$ of the propagating waves (see Fig. 3 in [25]). As a result, increases in the self-amplitude modulation (SAM) along with self-phase modulation (SPM) and self-focusing are satisfied. The SPM generates exploitable extra bandwidth between the modeless beating waves. Together with the relatively more optimized net GVD in the first setup (Table 1) justifies the attainment of better spectral width values. This agrees well to the simulation in [18] that described the favourable properties for spectral broadening with the improvement in Kerr-nonlinearity, γ and the minimization in fiber dispersion, β_2. With the strengthening of γ induced by the tighter geometry also results in the initiation and stabilization of the "SBE" as well as the "WS" states. For the latter, its common trait to that of "UWS" was almost nice and smooth spectral shapes without Kelly sidebands (Figs. 4, 5 and 8).

Table 4. Summary of lasing characteristics at different configurations.

Parameters	Setup 1: Fig. 3	Setup 2: Fig. 7
Fiber-geometry	Tighter confinement (stronger γ)	All ordinary SMF fiber (weaker γ)
Output power flow	Almost quadratic fit.	Almost linear fit.
Wave kinetics response	Smoother trendline for "SBE" state from 1.76 to 3.53nm band	Overall ups and down from 1.58nm to 3.53nm as well as-suffering saturation.
"WS" & "UWS" states	Stable zone, BW range= 4.05 to 4.88nm. η = 21% to 23%	Unstable zone, max. BW~ 4.25nm. Difficult to maintain this state.

In solid-state lasers (SSLs), a tight crystal to mirror length tolerance is needed for the optimization of γ [see Fig. 3(a) in (28)]. Once this is satisfied, instabilities to CW power operation is initiated which is comparable to "UWS" state in this laser scheme. Further adjustment of the free-space optics together with a small mechanical perturbation lead to stable operation. This is similar to the realization of "WS" in this report that requires no necessity for physical or optical adjustment. Although involving only a small power segment, this was just the first step that inspires a more promising scientific breakthrough. We only introduce analogy to SSLs but do not claim of any presence of some strict stability map in random lasers. Due to our lack of expertise and facilities, this text also does not cover the behaviours of optical rogue waves presented in [16] that might hints the underlying physics behind "WS" and "UWS" states formation. The main scopes are on the exceptional spectral growth characteristics and stabilization at low power scaling by including discussions on a fraction of commonly known nonlinear fiber optics theories. More investigations and mathematical analysis need to be done in the future to gain better understanding of the insight

Preprint not peer reviewed

This preprint research paper has not been peer reviewed. Electronic copy available at: https://ssrn.com/abstract=4184332

behind this phenomenon. It should be stressed again that the nature of the experimental design itself, comprising no FBG permits the freedom of wave kinetics assisted spectral improvement from narrower to broader widths as clarified in Fig. 2. The tighter geometry eases and boosts the creations of all stable broadening states. In fact through multiple attemps, we ourselves have proven experimentally the repeatability and reliability of the results obtained.

4. Conclusions

We have demonstrated the evolution of nonlinear broadening at L-band under tighter geometry in a backward pumped-random fiber laser that has no any fixed reflector. With the maximum 6.3 times wider lasing bandwidth than that of the CW pump source implies the best broadening attainment in the world operating at only 290mW output power. We believe that this was influenced by the optical Kerr-effect, γ similar to those observed in solid-state lasers. The insight behind this fulfillment relates to the flexibility of various efficient path interactions of each photon induced by multiple Rayleigh scattering feedback along the longitudinal waveguide dimension. This attribute has not been fully exploited yet compared to the ease of modifying multiple lasing features in free-space bulk optics. Thus, more future advancements are planned by improving the counterbalance between the net GVD and higher nonlinearities, γ. For instance, the use of longer passive gain fiber where the correct DCF length is employed to minimize the net GVD towards zero. More than 10nm bandwidth is expected by maintaining the same type of pump source under the right pumping distributions. Inspired by the long time understanding of Kerr-lensing in solid-state lasers, the results represent a basis for exploring the realization of hybrid solid-state and fiber laser traits in a single device footprint. This signifies the future aim of constructing a reliable, functional and optimized spectral performances of a single random fiber laser system, but having both combinations of solid-state and fiber laser properties. The waveguide structure eliminates the utilization of any additional optical elements in a free-space configuration that requires complicated cavity alignment and special care for cleaning procedures. No housing is required which simplifies the laser construction and maintenance. The system also satisfies turn-key operation with the immunity to tough environmental changes. A fiber laser looks and operates just like other electronic instruments where access is not required as the device will stay aligned for the entire lifetime. Under the precondition that external mode-locking modulations are implemented in this cavity-free structure, further utilization of this method might assist in improving the formation of ultrashort pulses even at low power levels.

Acknowledgements

This work was funded in part by the Ministry of Higher Education Malaysia under the Fundamental Research Grant Scheme (FRGS/1/2018/STG02/UPM/02/8). Thanks to David W Peckham and Howard Trieu from OFS Optics for their invaluable contributions to advise us on the technical properties of the fibers.

References

[1] S.K. Turitsyn, S.A. Babin, A.E. El-Taher, P. Harper, D. V. Churkin, S.I. Kablukov, J.D. Ania-Castañón, V. Karalekas, E. V. Podivilov, Random distributed feedback fibre laser, Nat. Photonics. 4 (2010) 231–235. https://doi.org/10.1038/nphoton.2010.4.

Preprint not peer reviewed

This preprint research paper has not been peer reviewed. Electronic copy available at: https://ssrn.com/abstract=4184332

[2] D. V. Churkin, S.A. Babin, A.E. El-Taher, P. Harper, S.I. Kablukov, V. Karalekas, J.D. Ania-Castañón, E. V. Podivilov, S.K. Turitsyn, Raman fiber lasers with a random distributed feedback based on Rayleigh scattering, Phys. Rev. A. 82 (2010) 033828. https://doi.org/10.1103/PhysRevA.82.033828.

[3] A.R. Sarmani, M.H. Abu Bakar, A.A.A. Bakar, F.R.M. Adikan, M.A. Mahdi, Spectral variations of the output spectrum in a random distributed feedback Raman fiber laser, Opt. Express. 19 (2011) 14152. https://doi.org/10.1364/OE.19.014152.

[4] W.L. Zhang, Y.J. Rao, J.M. Zhu, Z.X.Y. Wang, Zi Nan, X.H. Jia, Low threshold 2^nd-order random lasing of a fiber laser with a half-opened cavity, Opt. Express. 20 (2012) 14400. https://doi.org/10.1364/OE.20.014400.

[5] S.A. Babin, A.E. El-Taher, P. Harper, E. V. Podivilov, S.K. Turitsyn, Tunable random fiber laser, Phys. Rev. A. 84 (2011) 021805. https://doi.org/10.1103/PhysRevA.84.021805.

[6] D. V. Churkin, S. Sugavanam, I.D. Vatnik, Z. Wang, E. V. Podivilov, S.A. Babin, Y. Rao, S.K. Turitsyn, Recent advances in fundamentals and applications of random fiber lasers, Adv. Opt. Photonics. 7 (2015) 516. https://doi.org/10.1364/AOP.7.000516.

[7] S.K. Turitsyn, S.A. Babin, D. V. Churkin, I.D. Vatnik, M. Nikulin, E. V. Podivilov, Random distributed feedback fibre lasers, Phys. Rep. 542 (2014) 133–193. https://doi.org/10.1016/j.physrep.2014.02.011.

[8] A.R. Sarmani, M.H. Abu Bakar, F.R. Mahamd Adikan, M.A. Mahdi, Laser Parameter Variations in a Rayleigh Scattering-Based Raman Fiber Laser With Single Fiber Bragg Grating Reflector, IEEE Photonics J. 4 (2012) 461–466. https://doi.org/10.1109/JPHOT.2012.2190925.

[9] D. V. Churkin, I. V. Kolokolov, E. V. Podivilov, I.D. Vatnik, M.A. Nikulin, S.S. Vergeles, I.S. Terekhov, V. V. Lebedev, G. Falkovich, S.A. Babin, S.K. Turitsyn, Wave kinetics of random fibre lasers, Nat. Commun. 6 (2015) 6214. https://doi.org/10.1038/ncomms7214.

[10] I.D. Vatnik, D. V. Churkin, S.A. Babin, S.K. Turitsyn, Cascaded random distributed feedback Raman fiber laser operating at 12 μm, Opt. Express. 19 (2011) 18486. https://doi.org/10.1364/OE.19.018486.

[11] I.D. Vatnik, D. V. Churkin, S.A. Babin, Spectral width optimization in random DFB fiber laser, in: 2013 Conf. Lasers Electro-Optics Eur. Int. Quantum Electron. Conf. CLEO Eur., IEEE, 2013: pp. 1–1. https://doi.org/10.1109/CLEOE-IQEC.2013.6801369.

[12] D. V. Churkin, I.D. Vatnik, S.K. Turitsyn, S.A. Babin, Random distributed feedback Raman fiber laser operating in a 1.2 μm wavelength range, Laser Phys. 21 (2011) 1525–1529. https://doi.org/10.1134/S1054660X11150047.

[13] S.A. Babin, E.A. Zlobina, S.I. Kablukov, E. V. Podivilov, High-order random

Preprint not peer reviewed

This preprint research paper has not been peer reviewed. Electronic copy available at: https://ssrn.com/abstract=4184332

Raman lasing in a PM fiber with ultimate efficiency and narrow bandwidth, Sci. Rep. 6 (2016) 22625. https://doi.org/10.1038/srep22625.

[14] J. Xu, Z. Lou, J. Ye, J. Wu, J. Leng, H. Xiao, H. Zhang, P. Zhou, Incoherently pumped high-power linearly-polarized single-mode random fiber laser: experimental investigations and theoretical prospects, Opt. Express. 25 (2017) 5609. https://doi.org/10.1364/OE.25.005609.

[15] B.C. Yao, Y.J. Rao, Z.N. Wang, Y. Wu, J.H. Zhou, H. Wu, M.Q. Fan, X.L. Cao, W.L. Zhang, Y.F. Chen, Y.R. Li, D. Churkin, S. Turitsyn, C.W. Wong, Graphene based widely-tunable and singly-polarized pulse generation with random fiber lasers, Sci. Rep. 5 (2016) 18526. https://doi.org/10.1038/srep18526.

[16] J. Xu, J. Wu, J. Ye, J. Song, B. Yao, H. Zhang, J. Leng, W. Zhang, P. Zhou, Y. Rao, Optical rogue wave in random fiber laser, Photonics Res. 8 (2020) 1. https://doi.org/10.1364/PRJ.8.000001.

[17] J. Dong, L. Zhang, J. Zhou, W. Pan, X. Gu, Y. Feng, More than 200 W random Raman fiber laser with ultra-short cavity length based on phosphosilicate fiber, Opt. Lett. 44 (2019) 1801. https://doi.org/10.1364/OL.44.001801.

[18] S. V. Smirnov, D. V. Churkin, Modeling of spectral and statistical properties of a random distributed feedback fiber laser, Opt. Express. 21 (2013) 21236. https://doi.org/10.1364/OE.21.021236.

[19] S.A. Babin, D. V. Churkin, A.E. Ismagulov, S.I. Kablukov, E. V. Podivilov, Turbulence-induced square-root broadening of the Raman fiber laser output spectrum, Opt. Lett. 33 (2008) 633. https://doi.org/10.1364/OL.33.000633.

[20] S.A. Babin, D. V. Churkin, A.E. Ismagulov, S.I. Kablukov, E. V. Podivilov, Four-wave-mixing-induced turbulent spectral broadening in a long Raman fiber laser, J. Opt. Soc. Am. B. 24 (2007) 1729. https://doi.org/10.1364/JOSAB.24.001729.

[21] S.A. Babin, D. V. Churkin, A.E. Ismagulov, S.I. Kablukov, E. V. Podivilov, Spectral broadening in Raman fiber lasers, Opt. Lett. 31 (2006) 3007. https://doi.org/10.1364/OL.31.003007.

[22] J. Xu, J. Ye, W. Liu, J. Wu, H. Zhang, J. Leng, P. Zhou, Passively spatiotemporal gain-modulation-induced stable pulsing operation of a random fiber laser, Photonics Res. 5 (2017) 598. https://doi.org/10.1364/PRJ.5.000598.

[23] W. Pan, L. Zhang, H. Jiang, X. Yang, S. Cui, Y. Feng, Ultrafast Raman fiber Laser with Random Distributed Feedback, Laser Photon. Rev. 12 (2018) 1700326. https://doi.org/10.1002/lpor.201700326.

[24] D.E. Spence, P.N. Kean, W. Sibbett, 60-fsec pulse generation from a self-mode-locked Ti:sapphire laser, Opt. Lett. 16 (1991) 42.

Preprint not peer reviewed

This preprint research paper has not been peer reviewed. Electronic copy available at: https://ssrn.com/abstract=4184332

https://doi.org/10.1364/OL.16.000042.

[25] U. Keller, Recent developments in compact ultrafast lasers, Nature. 424 (2003) 831–838. https://doi.org/10.1038/nature01938.

[26] Q. Kuang, L. Zhan, Z. Gu, Z. Wang, High-Energy Passively Mode-Locked Raman Fiber Laser Pumped by a CW Multimode Laser, J. Light. Technol. 33 (2015) 391–395. https://doi.org/10.1109/JLT.2014.2375339.

[27] Q. Kuang, L. Zhan, Z. Wang, M. Huang, Up to the 1552nd Order Passively Harmonic Mode-Locked Raman Fiber Laser, IEEE Photonics Technol. Lett. 27 (2015) 2205–2208. https://doi.org/10.1109/LPT.2015.2457238.

[28] A.A. Lagatsky, C.T.A. Brown, W. Sibbett, Highly efficient and low threshold diode-pumped Kerr-lens mode-locked Yb:KYW laser, Opt. Express. 12 (2004) 3928. https://doi.org/10.1364/OPEX.12.003928.

[29] V. Karalekas, J.D. Ania-Castañón, P. Harper, S.A. Babin, E. V. Podivilov, S.K. Turitsyn, Impact of nonlinear spectral broadening in ultra-long Raman fibre lasers, Opt. Express. 15 (2007) 16690. https://doi.org/10.1364/OE.15.016690.

[30] Y. Tang, J. Xu, A random Q-switched fiber laser, Sci. Rep. 5 (2015) 9338. https://doi.org/10.1038/srep09338.

Preprint not peer reviewed

This preprint research paper has not been peer reviewed. Electronic copy available at: https://ssrn.com/abstract=4184332